

See discussions, stats, and author profiles for this publication at: <https://www.researchgate.net/publication/231684368>

Structural study of polyethers on graphite by scanning tunneling microscopy. Polymerization-induced epitaxy

ARTICLE *in* MACROMOLECULES · DECEMBER 1992

Impact Factor: 5.8 · DOI: 10.1021/ma00051a037

CITATIONS

25

READS

6

3 AUTHORS, INCLUDING:



Darryl Y Sasaki

Sandia National Laboratories

148 PUBLICATIONS 3,188 CITATIONS

[SEE PROFILE](#)



Toyoki Kunitake

FAIS

672 PUBLICATIONS 21,140 CITATIONS

[SEE PROFILE](#)

Structural Study of Polyethers on Graphite by Scanning Tunneling Microscopy. Polymerization-Induced Epitaxy

Masahito Sano,^{*†} Darryl Y. Sasaki,[‡] and Toyoki Kunitake[§]

Molecular Architecture Project—JRDC, Kurume Research Park, Kurume, Fukuoka 830, Japan

Received June 24, 1992; Revised Manuscript Received September 8, 1992

ABSTRACT: The newly found phenomenon of polymerization-induced epitaxy can produce an ultrathin film of highly oriented polymer molecules on a solid surface. Poly(tetrahydrofuran), poly(oxacyclobutane), and poly(ethylene oxide) were epitaxially grown on the basal plane of graphite via *in situ* polymerization and their intra- and interchain structures as well as epitaxial orientations were examined by scanning tunneling microscopy (STM). STM images indicated these polymer chains in a planar, all trans conformation commensurate with the graphite lattice. Different polymer lattices can be constructed by mutually shifting a chain with respect to the adjacent chain along the backbone direction, in units of the graphite hexagon. Most of the STM images can be explained by moiré patterns generated through rotations of the polymer lattice on top of the graphite lattice. Such a pattern can only be observed if the film exists as a monolayer. Furthermore, we find that the present epitaxial growth process proceeds such that the two-dimensional array that constitutes a basic repeating pattern of a fringe, defined by the number of structural repeating units along the polymer backbone and the number of chains within a commensurate cell, becomes the first two smallest of all other possibilities, namely, one unit, one chain or seven units, seven chains.

Introduction

Polymerization-induced epitaxy is defined as the synthesis of polymeric molecules in the presence of a solid substrate where the resulting polymer on the solid surface has a structure that is strongly influenced by the atomic arrangement of the substrate surface.¹ Since a polymeric molecule consists of many repeating units, the epitaxial structure may reside within a molecular chain as well as between the polymer molecules. This implies that the epitaxial process can be used to orient macromolecules on the surface with each repeating unit arranged within a two-dimensional order. Taking advantage of different physical properties of the epitaxially grown polymers from the analogous polymer in the bulk, an ultrathin film of a two-dimensionally ordered structure can be obtained by simple washing techniques.

Previously, two methods were known to prepare epitaxially grown polymeric materials. The most frequently used method is the epitaxial crystallization of preformed polymers from solution or the melt.^{2,3} The other technique employs the topochemical solid-state polymerization, which has been referred to as epitaxial polymerization in some cases.⁴ The latter technique involves a formation of a crystal film by the epitaxial crystallization of the monomer, followed by the solid-state polymerization of the monomer crystal. We reserve the term "epitaxially polymerized materials" to the compounds formed by the method of polymerization-induced epitaxy where epitaxy occurs during the polymerization process itself, yielding the epitaxially oriented polymer directly on the surface.

These previous studies were based on optical microscopic observations, unit cell analyses of diffraction experiments, or the contact film method of three dimensionally grown epitaxial crystals. They indicate that the lattice matching of polymer crystals and the substrate surface is not as crucial as that of low-molecular-weight molecules. How-

ever, an exact orientation of polymer molecules with respect to the substrate surface remained mostly unknown.

Recently, scanning tunneling microscopy (STM) has been successfully applied to structural analyses of organic adsorbates on a conducting substrate. In the case of liquid crystals⁵ and alkylated compounds,^{6,7} quality of images is sufficient to argue an adsorbate registry with the substrate surface at the atomic level. Nevertheless, one must be careful in analyzing molecular images in general, since the contrast mechanism of organic adsorbates are not known to predict the actual feature of adsorbate images.^{8,9}

We have succeeded in epitaxially polymerizing polyethers on the graphite surface by conventional ring-opening reactions,¹⁰ producing molecularly thin films after washing away the bulk materials. Fourier transform infrared spectroscopy (FTIR) and X-ray photoelectron spectroscopy (XPS) were used to identify the resulting films on graphite. Epitaxial structures of the polymer film were directly probed by STM. A preliminary account of epitaxially grown polyether films on graphite has been reported earlier.¹

Various polymerization conditions were surveyed to determine the generality of this phenomenon. Also, by analysis of a set of polyethers from monomers varying in ring size, characteristic aspects of the STM images could be distinguished readily and less ambiguously. The linear, symmetrical, and simple atomic composition (O, C, H) of these polymers allows for straightforward modeling and interpretation of the imaged structures. Various moiré patterns generated by a monolayer of the polymer sheet and the bare graphite lattice show, for the first time, the epitaxial orientations of the polymeric molecules with respect to the graphite lattice in atomic detail.

Experimental Section

General Procedure. All polymerizations were conducted in oven-dried glassware under N₂ atmosphere. Tetrahydrofuran was refluxed over Na and then distilled. Oxacyclobutane (Aldrich) was refluxed over CaH₂ and distilled prior to use. Ethylene oxide (Kodak) and the initiators trifluoromethanesulfonic anhydride (Wako Chemical), boron trifluoride etherate (Wako Chemical), and triethylxonium tetrafluoroborate (1.0 M in dichloromethane, Aldrich) were all used as received. Highly

^{*} Present address: π-Electron Materials Project—JRDC, 43 Miyukigaoka, Tsukuba, Japan.

[†] Present address: Department of Chemical Engineering, California Institute of Technology, Pasadena, CA.

[‡] Present address: Department of Chemical Science and Technology, Faculty of Engineering, Kyushu University, Fukuoka, Japan.

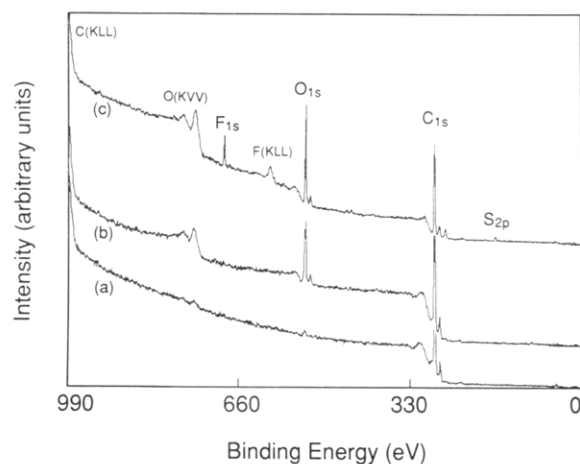


Figure 1. XPS spectra of (a) bare HOPG, (b) epitaxial film of PTHF on HOPG initiated by $(CF_3SO_2)_2O$, and (c) bulk materials of polymerization of (b) cast on HOPG.

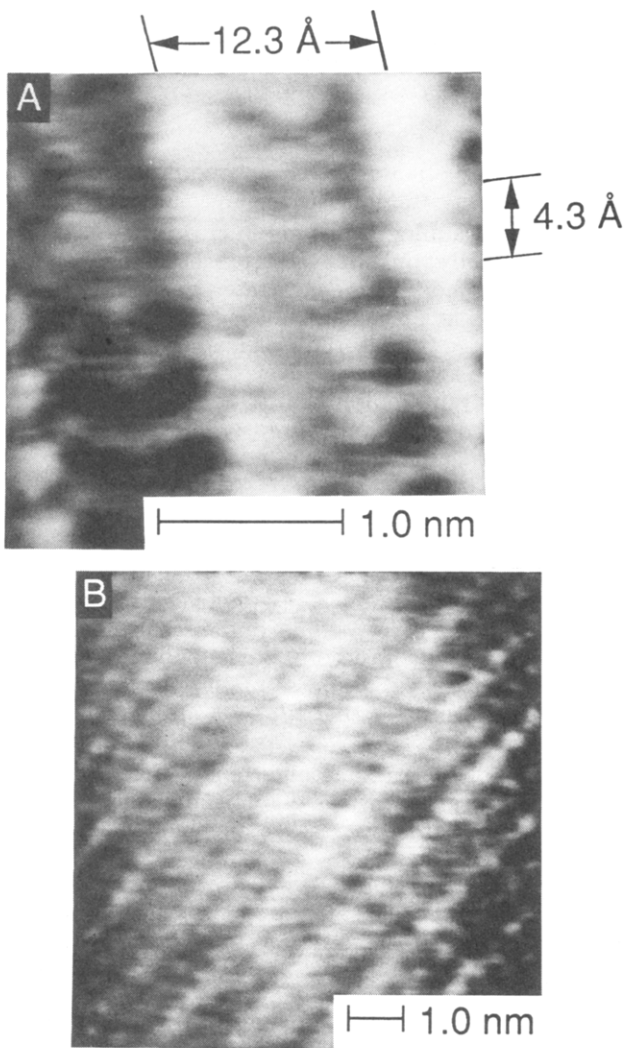


Figure 2. STM images of PTHF on HOPG in high resolution (A) and wide scan (B) modes, taken at the different locations. These images are classified as PTHF-I- 0° . The distances indicated on this and following figures are measured perpendicular to the periodic arrays of the bright regions.

oriented pyrolytic graphite (HOPG) having a dimension of $10 \times 25 \times 2$ mm³ was obtained from Union Carbide.

Poly(tetrahydrofuran) (PTHF). For the cationic ring-opening polymerization of poly(tetrahydrofuran) (PTHF), three different initiators were used: $(CF_3SO_2)_2O$ involving a super acid,¹¹ a preformed oxonium ion of $(C_2H_5)_3O^+(BF_4)^-$,¹² and a Lewis acid $BF_3O(C_2H_5)_2$.¹³

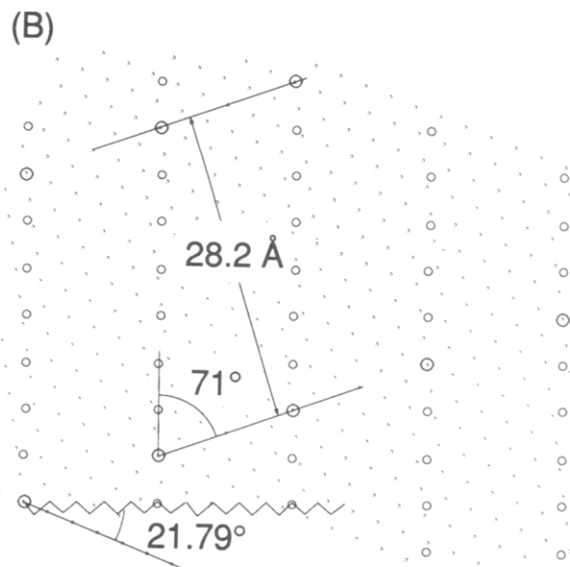
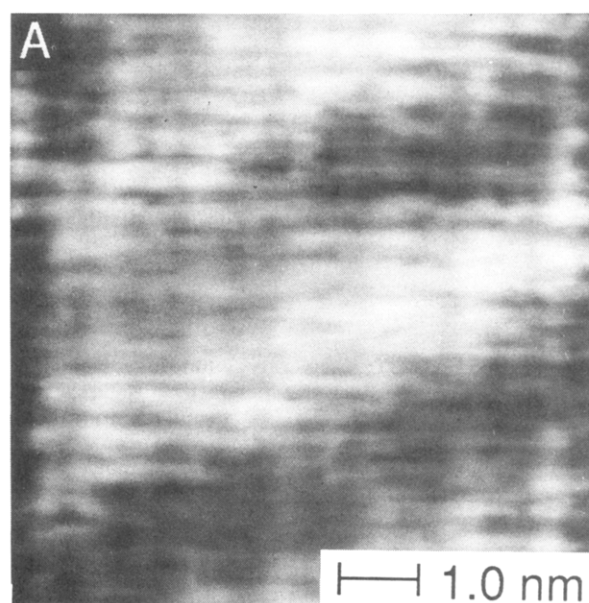


Figure 3. (A) An STM image of PTHF on HOPG exhibiting a moiré pattern. (B) A schematic drawing of PTHF-I- 21.79° . In this and the following schematic drawings, a small dot represents a bright node of the graphite hexagonal lattice. Superimposed on this lattice is a STM polymer lattice with the relevant ether oxygen denoted by a circle. The node where these two circles match is associated with the region of a bright fringe by the assumptions made for STM contrast and is indicated by a larger circle. The zigzag line is drawn to show the polymer chain direction.

Into neat THF (10 mL) was placed freshly cleaved HOPG followed by addition of the initiator (3–5 drops), and the mixture was swirled several times to allow mixing. (Reversing the order of the addition of initiator and HOPG in the THF does not affect the final result.) After 12 h at room temperature, ethanol was added and the solid mass was heated slightly to allow solvation of the polymer, thus liberating the HOPG plate. HOPG was washed thoroughly with THF and ethanol. In all cases, the bulk polymer typically had a weight averaged molecular weight (M_w) of 38 000 with a polydispersity index (p.d.) of less than 1.2 as estimated from gel permeation chromatography.

Poly(oxacyclobutane) (POCB). Oxacyclobutane (3 mL) was diluted with dry CH_2Cl_2 (3 mL), and HOPG was immersed in the solution. The reaction vessel was cooled to $-63^\circ C$, then initiated with $(C_2H_5)_3O^+(BF_4)^-$ solution (5 mol %). After 3 h at $-63^\circ C$ the mixture was allowed to equilibrate to room temperature. After 12 h the reaction was quenched with ethanol and the HOPG taken out and then rinsed with CH_2Cl_2 and ethanol, repeatedly.

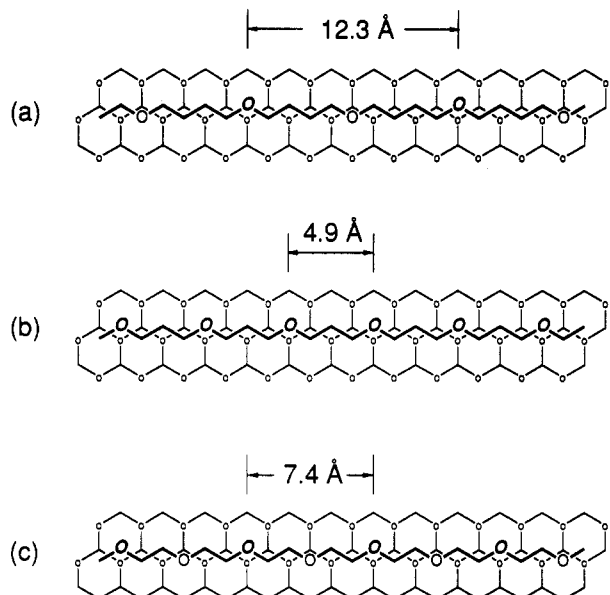


Figure 4. Graphite-polymer epitaxial structures of (a) PTHF, (b) POCH, and (c) PEO. A small circle on the graphite hexagonal lattice indicates a predominant tunneling site in STM. Due to the all trans conformation, every other oxygen of PTHF and PEO is equivalent, shown as bold letters in these figures.

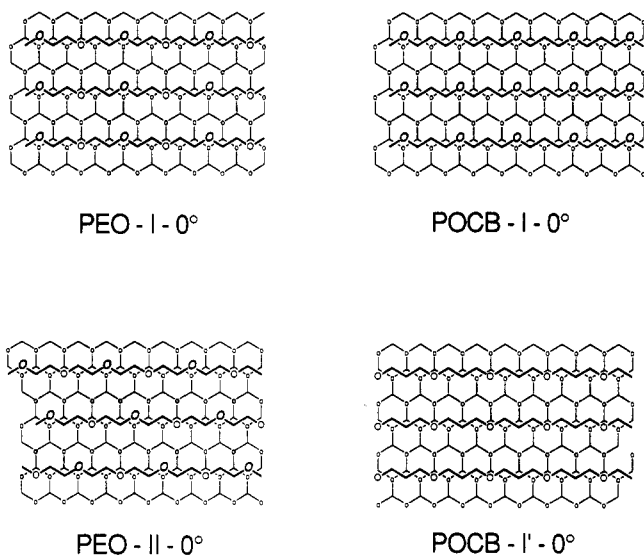


Figure 5. Different intermolecular structures of polymer sheets. The graphite hexagonal lattice is also drawn for relative orientation. The last suffix 0° indicates that the polymer backbone runs along a row of the graphite hexagonal cells without any rotation.

The bulk polymer had $M_w = 6000$ with p.d. = 2.3 with residual oligomers detected.

Poly(ethylene oxide) (PEO). Similar conditions as those for POCH using ethylene oxide monomer with $\text{BF}_3\text{O}(\text{C}_2\text{H}_5)_2$ as the initiator were followed. The bulk polymer had $M_w = 800$ with p.d. = 2.0 and residual oligomers were present.

Analysis of Polymer-Coated Graphite. All measurements of FTIR (Nicolet 710), XPS (Perkin-Elmer PHI 5300 ESCA system), and STM¹⁴ were conducted on the same sample. The STM was operated in air at ambient condition using Pt/Ir as a tip. Typically, the current was set at about 200 pA with a bias of 0.2–1 V. No particular difference was observed on the images with the polarity or the magnitude of bias voltage. If the bias voltage was reduced to less than about 0.1–0.2 V, the polymer image became unstable and would occasionally be lost irreversibly. In some cases, the underlying graphite could be seen. The variable current mode yielded five to six images every second, which were stored in the video. A summed image from about 1-s duration of video was transferred to a computer. Since our STM image was made directly from the preamp output without any external

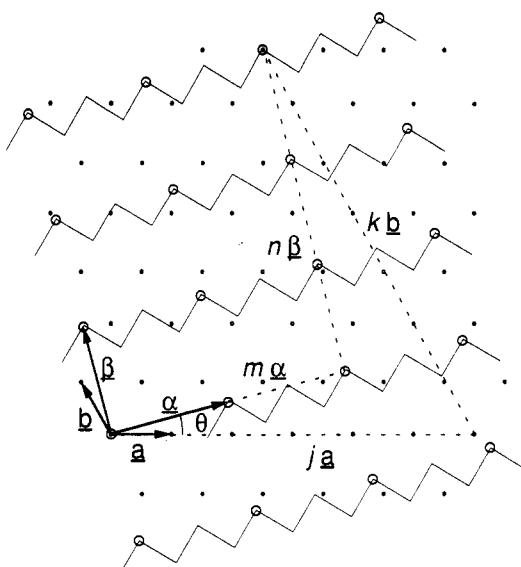


Figure 6. Geometry of the basis vectors, $\{a, b\}$ for graphite and $\{\alpha, \beta\}$ for polymers, respectively. The graphite lattice is represented by a small dot. The zigzag lines denote the polymer chains with a large circle signifying the relevant ether oxygens on the chain. Taking an origin to be one of the matching nodes, a rotation of the polymer lattice by θ brings another polymer node on top of the graphite node at (j, k) in the graphite coordinate or (m, n) in the polymer space.

filter, it usually contained high-frequency noises as well as inclined baselines. The final image was low-pass filtered but was not corrected for the baseline.

Results and Discussion

Chemical Identification. FTIR spectra in the reflection mode of all polyether samples on HOPG had poor signal-to-noise ratios because of the small quantity of highly oriented polymer molecules on the surface. Also, interfering peaks due to atmospheric water and CO_2 in the regions above 3300 cm^{-1} and below 2000 cm^{-1} made peak assignments difficult. Thus, although every sample showed peaks at ca. 2950 and 2870 cm^{-1} indicating the presence of aliphatic chain C–H stretching, the C–O ether stretching around 1100 cm^{-1} was difficult to discern.

Therefore, XPS was applied to identify the polymer. XPS could also detect for residual initiators on the HOPG surface, since it might be possible that STM images were caused by an artifact produced by the initiator reacting with graphite. Figure 1b shows the XPS spectrum of the PTHF-HOPG sample polymerized by $(\text{CF}_3\text{SO}_2)_2\text{O}$ initiator. Also shown are spectra of (a) the bare HOPG and (c) the HOPG covered by a cast of bulk materials from the reaction mixture. Clearly, the O_{1s} peak of the PTHF-HOPG sample increased substantially compared with the bare HOPG. In addition, there were no measurable peaks corresponding to F_{1s} and S_{2p} of the initiator compared with O_{1s} peak. Similar spectra were obtained for other PTHF samples, POCH-HOPG and PEO-HOPG samples with no detection of initiators including B_{1s} . These data strongly support that only polymer films remained on the HOPG surface after repeated washing by good solvents for the bulk polymers. Consistent with this is the observation that STM images of the polymers were independent of initiators.

STM Contrast. Figures 2 and 3A show some examples of the STM images of PTHF. In Figure 2, the array of bright atoms has a long periodicity of 12.3 \AA (in the horizontal direction in this image) and a short periodicity of 4.3 \AA . A moiré pattern is visible in the image of Figure 3A. A brighter region corresponds to a stronger current

Table I
Selected Rotational Angles for Moiré Fringes^a

PTHF ($\alpha = 5a$)			
PTHF-I ($\psi = 0^\circ, \beta = \sqrt{3}a$)		PTHF-II ($\psi = 30^\circ, \beta = 2a$)	
θ (deg)	$m = 0$ $n(j,k)$	$m = 1$ $n(j,k)$	$m = 0$ $n(j,k)$
21.79	7 (2,13)	1 (6,4)	21.79
38.22	7 (-2,11)	-1 (6,2)	38.22
27.80	13 (1,23)	3 (6,8)	27.80
32.21	13 (-1,22)	-3 (6,2)	32.21
9.43	37 (26,73)	-2 (4,-3)	13.18
50.58	37 (-26,47)	2 (4,7)	42.11
			31 (-48,22)
			3 (1,6)
PTHF-III ($\psi = 49.1^\circ, \beta = \sqrt{7}a$) PTHF-IV ($\psi = 66.59^\circ, \beta = \sqrt{19}a$)			
θ (deg)	$m = 0$ $n(j,k)$	$m = 1$ $n(j,k)$	$m = 0$ $n(j,k)$
21.79	1 (-2,1)		21.79
38.22	7 (-18,1)	3 (-2,4)	38.22
			7 (-34,-9)
			2 (-4,1)
PTHF-V ($\psi = 60^\circ, \beta = \sqrt{12}a$)			
θ (deg)	$m = 0$ $n(j,k)$	$m = 1$ $n(j,k)$	
21.79		7 (-22,4)	5 (-10,5)
38.22		7 (-26,-4)	1 (2,3)
POCB ($\alpha = 2a$)			
POCB-I ($\psi = 0^\circ, \beta = \sqrt{3}a$)		POCB-II ($\psi = 30^\circ, \beta = 2a$)	
θ (deg)	$m = 0$ $n(j,k)$	$m = 1$ $n(j,k)$	$m = 0$ $n(j,k)$
21.79	7 (2,13)	-1 (2,-1)	21.79
38.22	7 (-2,11)	1 (2,3)	38.22
27.80	13 (1,23)	-4 (2,-6)	27.80
32.21	13 (-1,22)	4 (2,8)	32.21
13.17	19 (11,37)	10 (8,20)	13.17
			19 (10,32)
			8 (-2,14)
PEO ($\alpha = 3a$)			
PEO-I ($\psi = 0^\circ, \beta = \sqrt{3}a$)		PEO-II ($\psi = 30^\circ, \beta = 2a$)	
θ (deg)	$m = 0$ $n(j,k)$	$m = 1$ $n(j,k)$	$m = 0$ $n(j,k)$
21.79	7 (2,13)	2 (4,5)	21.79
38.22	7 (-2,11)	-2 (4,-1)	38.22
13.17	19 (11,37)	-4 (1,-7)	32.21
46.83	19 (-11,26)	4 (1,8)	46.83
			19 (-32,10)
			-1 (5,2)

^a The parameters for STM graphite lattice are $a = b = a (= \sqrt{3}r)$, $\varphi = 30^\circ$. In general, these polyethers produce the solutions ($m = 0, n$) at $30^\circ \pm \omega$. These are given as $n = 7$ at $\omega = 8.22^\circ$, 13 at 2.20° , 19 at 16.82° , 31 at 12.11° , 37 at 20.58° , and so forth.

site in these gray-scale images. In order to analyze these STM images, we start with the following assumptions.

(1) Contrast of the ether oxygen atom is different from the aliphatic carbons of the polymer molecules. By observation of the high resolution images of these polymers, such as the one shown in Figure 2A, the oxygen atom is assumed to contribute stronger than the aliphatic carbons to the measured current.

(2) It is well-known that, with bare graphite, every other carbon atom of the graphite hexagon contributes to the tunneling current strongly. Thus, we may expect that contrast of an adsorbed atom in close vicinity of the predominantly tunneling graphite carbon is enhanced more than others that are away from it.

The second point has been already proposed with other alkylated compounds on graphite.⁶ This assumption follows from a more general idea that the tunneling microscope actually images the conducting graphite surface, while contrast of the image feature is modified by the presence of physisorbed molecules. Thus, the observed images need not be associated with an electronic structure of an isolated adsorbate molecule.

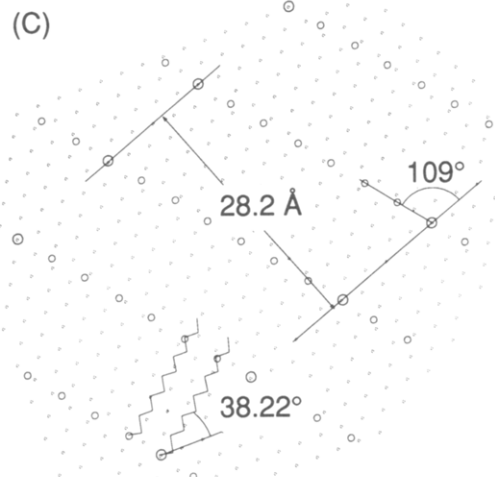
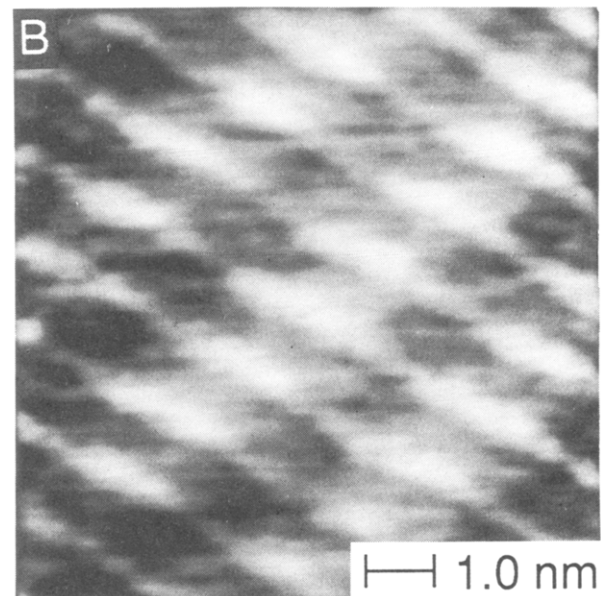


Figure 7. STM images (A, B) and a schematic drawing (C) of PTHF-I-38.22°. A wide scan image (B) shows bright fringes that are 28 Å apart. A high-resolution image (A) taken at the same location as (B) exhibits a complex feature that is difficult to recognize without the pattern analysis.

This has an important corollary that an observed polyether image can be recognized as a moiré pattern

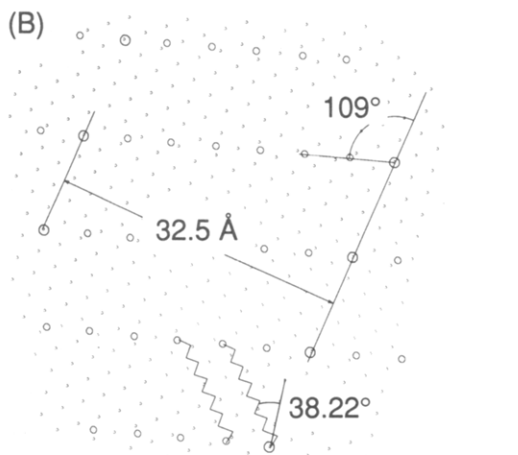
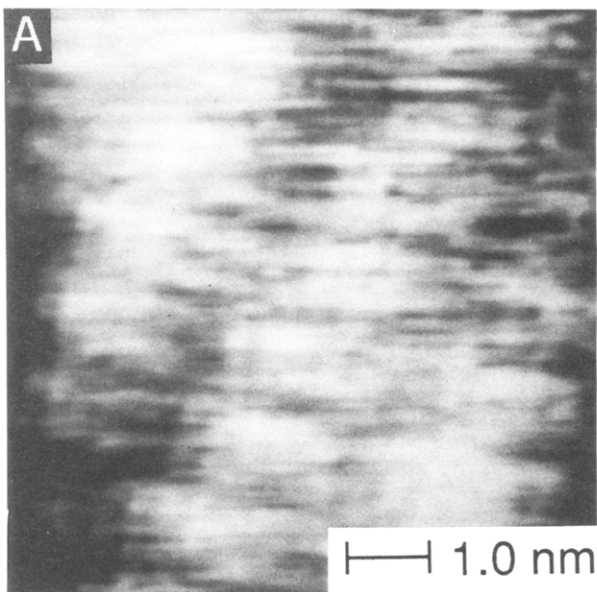


Figure 8. An STM image (A) and a schematic drawing (B) of PTHF-V-38.22.

generated from the graphite and the polymer lattices, provided that both lattices follow the above assumptions. It is important to note that the same polymer lattice can generate different moiré patterns depending on the relative orientation of the polymer lattice with respect to the graphite hexagonal lattice.

Intra- and Interchain Structure. The simplest intrachain structure that is consistent with the above assumptions and is common to many observed images is shown in Figure 4. All polymeric chains are characterized by the planar zigzag structures. This agrees with the calculated structure of polyethylene on graphite.¹⁵ Due to the all trans conformation, every other oxygen atom of PTHF and PEO is on the same line parallel to the chain skeleton and is equivalent from the STM point of view. An interesting consequence of this is that a basic unit relevant to STM images for POCH is shorter than one for PEO, although POCH has a longer chemical repeating unit than PEO. These extended planar forms are quite different from the bulk structures, where POCH and PEO are known to take helical forms.¹⁶ Bulk POCH and PEO can take a planar zigzag form only under special conditions such as inclusion of water molecules for POCH¹⁷ and mechanical tension for PEO.¹⁸ The proposed structures are invariant under a translation by the steps of one graphite hexagon unit of $a \equiv 2.46 \text{ \AA}$ ($=\sqrt{3}r$ where $r = 1.42 \text{ \AA}$ is the graphite carbon–carbon distance) along the chain direction with respect to the graphite lattice.

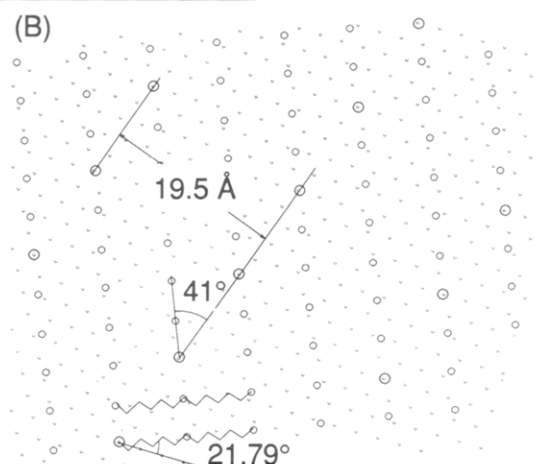
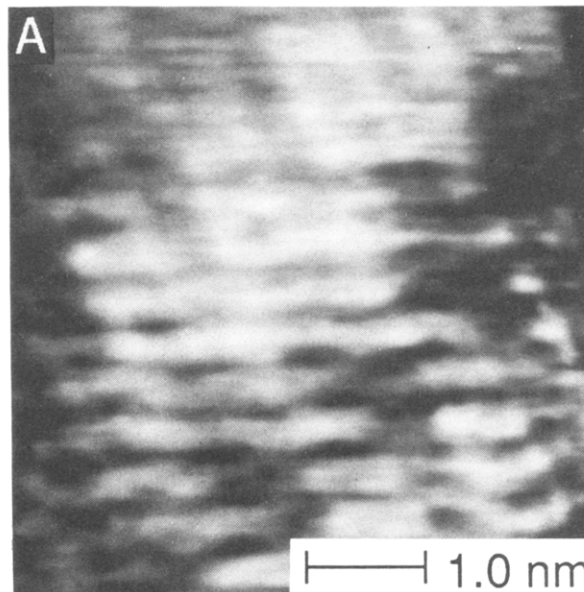


Figure 9. An STM image (A) and a schematic drawing (B) of PEO-I-21.79.

Most STM images contain a 4.3-Å spacing. This is taken as an intermolecular chain distance. This value also corresponds to the separation between every other graphite hexagon ($4.26 \text{ \AA} = 3r$). This epitaxial relation seems to hold for all type of samples. We can thereby construct different types of interchain packing by focusing on the relative position of oxygen atom with respect to the nearest neighbor chains.

Figure 5 shows some of the possible packing structures in the case of PEO and POCH. The graphite hexagonal lattice is also shown as a basic length unit. Type I has an oxygen atom of one chain directly below the oxygen of the next chain. Type II has the oxygen atom of one chain shifted by a to the right from the oxygen atom of the chain directly above, while the oxygen atom of type III would be shifted $2a$, and so on. For POCH, by translating the whole polymer sheet by $a/2$ would, while maintaining the relative atomic positions, bring every oxygen atom on top of the darker graphite carbon. This translated structure is denoted by placing a prime on the original structure and should be differentiated from the original structure on STM images. The perpendicular distance between the chains is fixed to 4.3 Å for all polymers, regardless of the structure type.

Epitaxial Orientation. Given a two-dimensional polymer lattice constructed as described, the observed STM images can be explained as moiré patterns produced

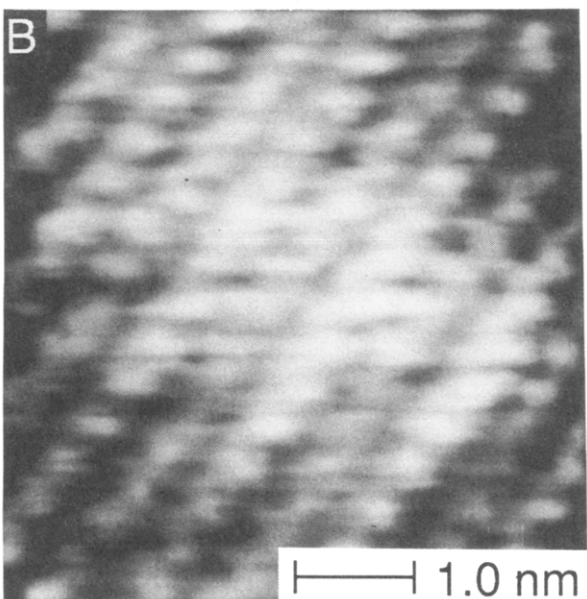
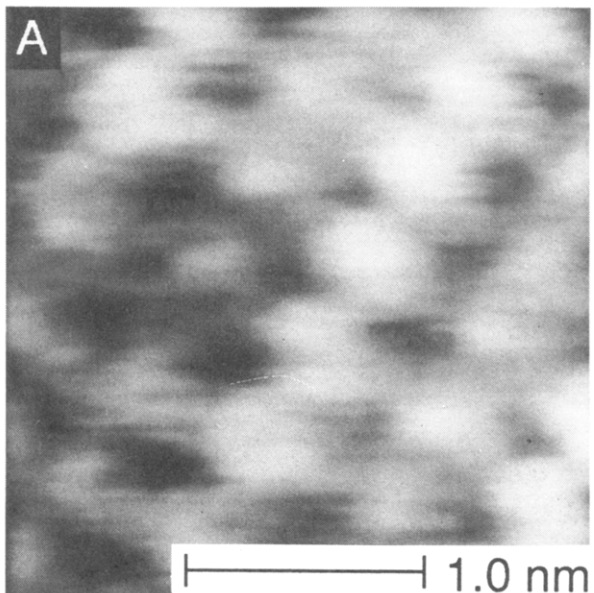


Figure 10. STM images of PEO-II-0° taken at the same location. The wide scan image (B) shows no fringe patterns.

by rotations of the polymer sheet with respect to the bare graphite image. According to the assumptions made on the STM contrast, the relevant polymer lattice is spanned by the position of equivalent oxygen atoms and the bare graphite lattice is described by every other carbon atom. We shall call these STM lattices in order to differentiate from the covalently bonded lattices.

Consider a relative rotation of a STM polymer lattice about the oxygen atom that matches with a graphite node. Since the polymer lattices proposed in Figure 5 are derived from the geometry based on the graphite hexagonal lattice, it is clear that there are numerous angles that some integer multiples of polymer nodes brings another oxygen atom on top of a graphite node.

Let $\{\mathbf{a}, \mathbf{b}\}$ and $\{\alpha, \beta\}$ be the nonorthogonal basis vectors of the STM graphite and polymer lattices, respectively. These basis vectors form the angles $(\pi/2 + \varphi)$ and $(\pi/2 + \Psi)$, respectively (Figure 6). We take α to be a vector from an oxygen atom to the next relevant oxygen along the backbone direction and β to be one from the original oxygen of the chain to a shifted oxygen of one chain directly above as a polymer lattice is constructed. The common origin

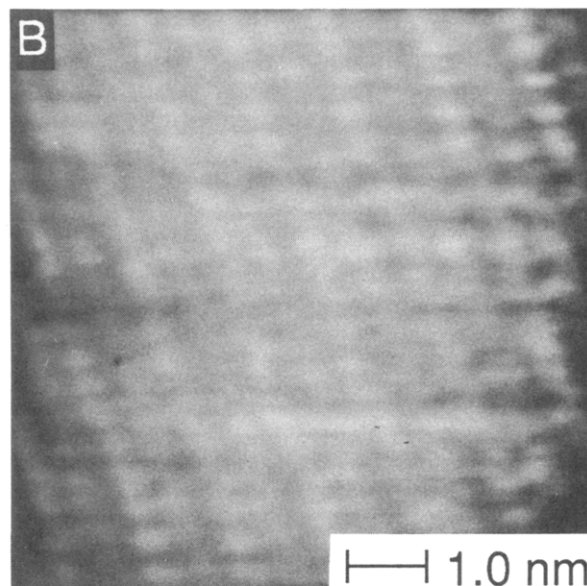
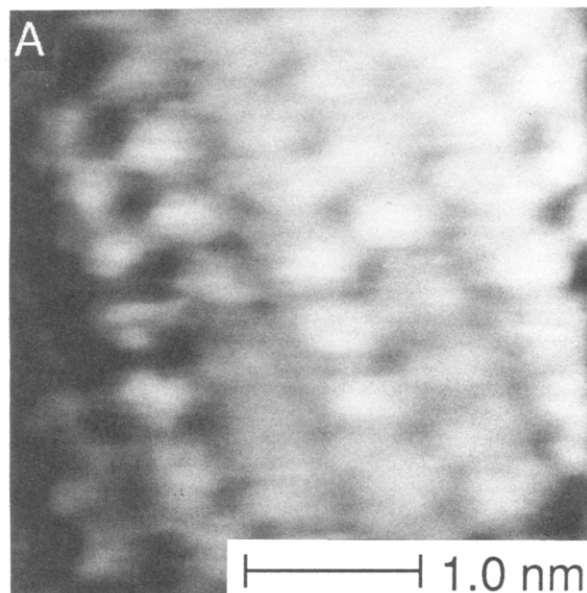


Figure 11. STM images of POCB-I-0°. The wide scan image (B) shows no fringe patterns.

is taken at the point where two nodes of each lattice overlap. A moiré pattern is generated by a rotation of the STM polymer lattice by an angle θ with respect to the STM graphite lattice, where θ is defined from \mathbf{a} to α . Then, the matching condition on θ is given by

$$m\alpha \cos \Psi = j\mathbf{a} \cos (\theta + \Psi) + k\mathbf{b} \sin (\theta + \Psi - \varphi)$$

and

$$n\beta \cos (\theta + \Psi) = k\mathbf{b} \cos \varphi - m\alpha \sin \theta \quad (1)$$

at $(m\alpha, n\beta)$ or $(j\mathbf{a}, k\mathbf{b})$ point, where m, n, k , and j are integers. The plain letter denotes the magnitude of a basis vector.

Equation 1 can be solved numerically for each structure type of polyethers. Table I summarizes selected integer pairs ($m = 0, n$) and ($m = 1, n$) in both coordinates at the angles of solution. We denote the epitaxial structure by (polymer)-(packing structure type)-(angle of rotation, θ) in this report. Because of the rotational symmetries of STM lattices concerned, there are numerous degenerate images. For instance, PTHF-II-(30° + ω) is a mirror image of PTHF-V-(30° - ω) and PTHF-III-(30° + ω) is related similarly to PTHF-IV-(30° - ω).

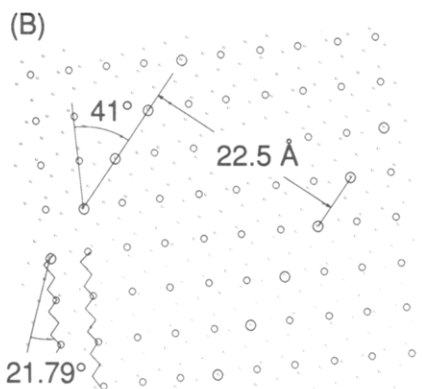
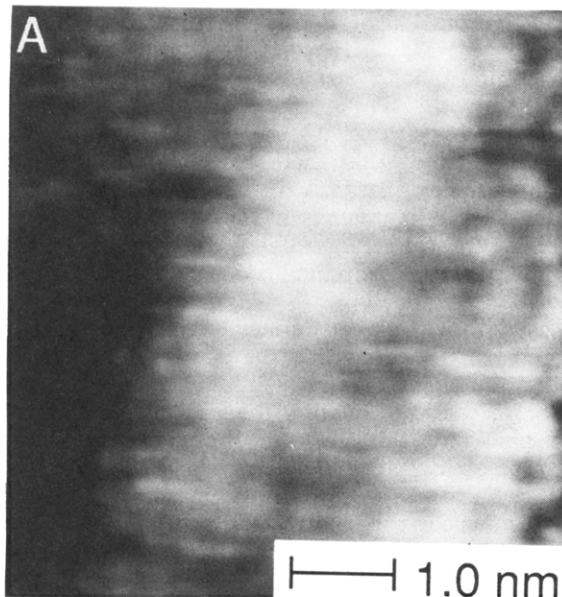


Figure 12. STM image (A) and a schematic drawing (B) of POCB-I-21.79°. The image appears brighter toward right, due to the tilted baseline which is not corrected.

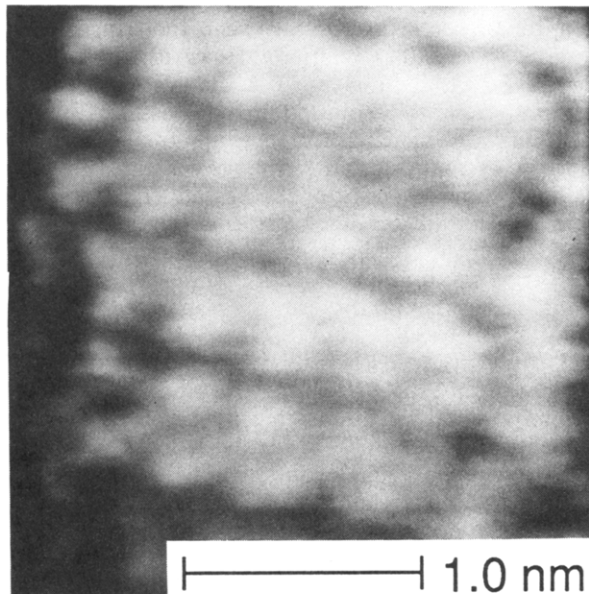


Figure 13. STM image that can be identified as either POCB-II-0° or POCB-II'-0°.

Figure 2 is then recognized as PTHF-I-0°. Images with $\theta = 0^\circ$ are the simplest to recognize, since these commensurate structures produce no moiré fringes and every polymer lattice node matches with the graphite node. These 0° images are consistent with our models of the

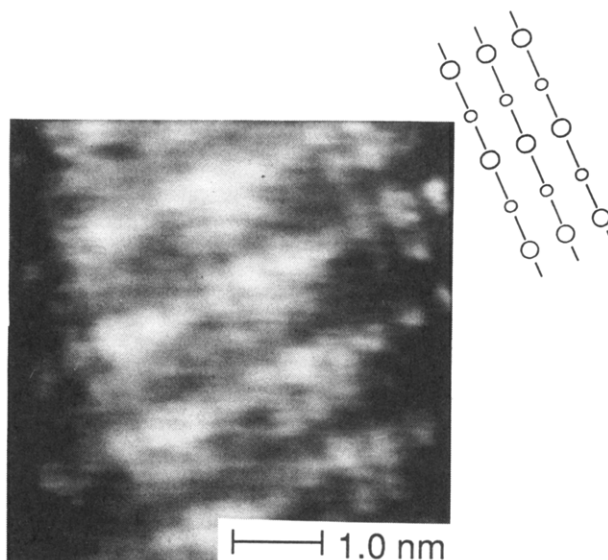


Figure 14. An image of PTHF in which the polymer structure is recognized as PTHF-I from the periodicity, but the moiré pattern does not correspond to any of the rotational models. The chain direction as shown in the schematic was identified by an agreement between the 12.3 Å distance between the bright spots and the model of Figure 4.

single chain structure of Figure 4 and the assumptions concerning the STM contrast.

Because detailed features of the observed image cannot be predicted with the present knowledge, our analysis is based on general appearance like the distance between bright troughs and angles formed by moiré fringes. By the second assumption, those nodes where the STM polymer lattice matches with the STM graphite lattice should appear brighter than other nodes and indicate the position of a bright fringe. This method is illustrated in the following images. The bright fringe visible in Figure 3A indicates this image to be PTHF-I-21.79°. This assignment is based on the observations that (1) the image has a distance between the bright fringes of 28.2 Å and that (2) the angle between the line of bright fringe and the line of oxygens in the β direction is 71°, as illustrated in a schematic drawing of Figure 3B. It is also interesting to note that the connecting lines of enhanced atoms are not associated with the actual polymer backbones.

We focus on these fringe characteristics for image assignments. Parts A and B of Figure 7 can be assigned as PTHF-I-38.22°, since they also have the fringe separation of 28.2 Å but the angle of 109°. Now, although PTHF-I-38.22° should be a mirror reflection of PTHF-I-21.79°, these images appear quite differently from the image of Figure 3A. Even though there are other images of PTHF-I-38.22° which have the exact feature of a mirror reflection of Figure 3A, we present these images of Figure 7 to demonstrate a difficulty of interpreting detailed features of the STM images in general.

Figure 8 shows an image of PTHF-V-38.22°, which is a mirror reflection of PTHF-II-21.79°. This epitaxial structure resembles PTHF-I-38.22° in that both have the bright fringe 109° inclined with respect to the β direction. However, the lines of enhancement are 28.2 Å apart for PTHF-I-38.22°, while being 32.5 Å apart for PTHF-V-38.22°.

Figures 9 and 10 exhibit PEO-I-21.79° and PEO-II-0°, respectively. The bright fringe of PEO-I-21.79° makes a 41° angle with β . PEO-II-0° is the most frequently observed image for PEO. POCB-I-0° and POCB-I-21.79° are shown in Figures 11 and 12. The POCB case is

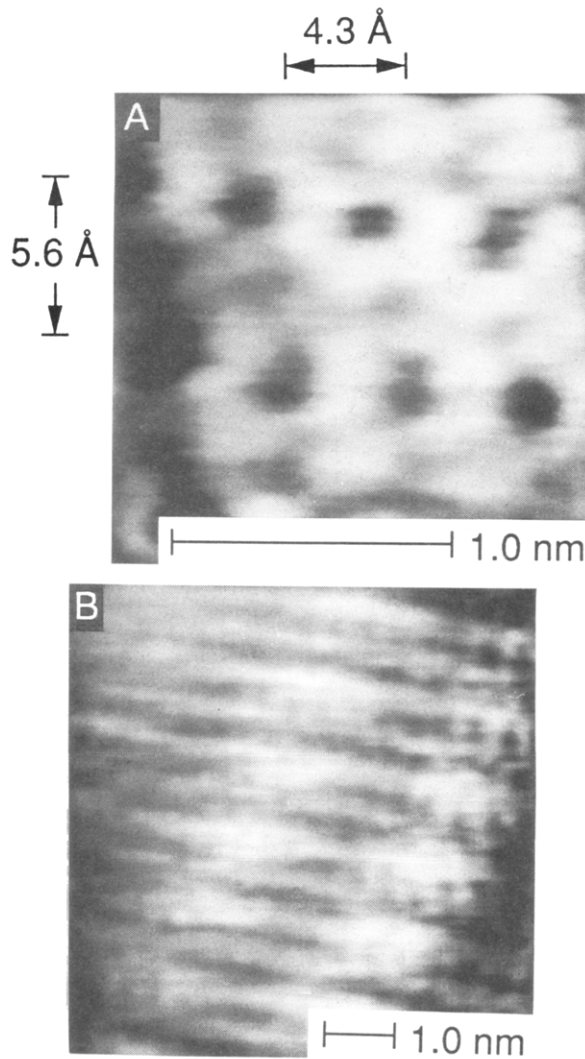


Figure 15. STM images of POCB that exhibit the patterns with the (0,7) relation as can be seen in (B), but also showing the short spacings of 5.6 Å in the high-resolution image of (A) that are not found in the polymer models.

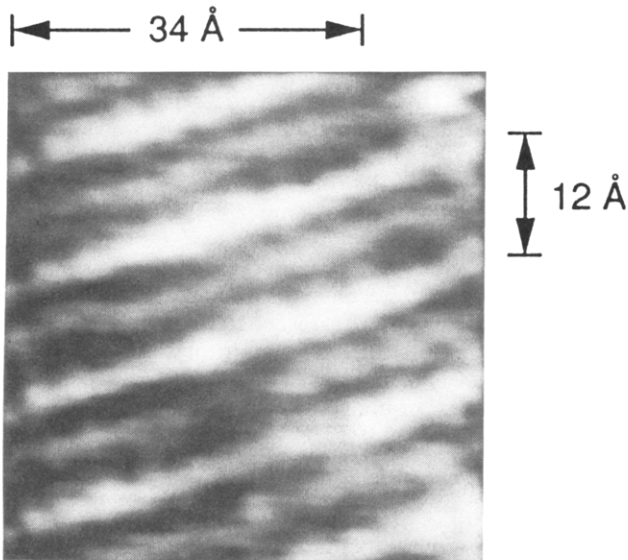


Figure 16. An image of PEO showing a pattern and a structure that is not explainable by the lattice rotational model.

complicated by not only $\alpha = 2\sqrt{3}r$ being close to $\beta = 3r$, but also a possible existence of type I' or II' structures which are difficult to interpret from the STM appearance.

Thus, Figure 13 can be identified as either POCB-II-0° or POCB-II'-0°.

It is important to note that those images that can be explained by this simple lattice rotational model, besides the $\theta = 0^\circ$ structure, have the ($m = 0, n = 7$) epitaxial relation, meaning that there are 7 chains between the matching nodes. Incidentally, the (0,7) relation always produces (7,0) matching in the direction of polymer backbone or seven structural repeating units on a polymer chain between the matching nodes. The epitaxial orientation characterized by (seven repeating units, seven chains) within a unit cell defined by the nearest neighbor matching nodes represents the smallest number of repeating units or chains in the unit cell. In other words, other than the $\theta = 0^\circ$ relation, the present epitaxial growth takes place such that the number of matching nodes per unit area on the polymer lattice is maximized.

Also, we notice that there is no single preferential structure type in these polyethers on graphite. Although we have not yet observed all conceivable structures, various types could be seen at different locations on the identical sample. Thus, the ether oxygen seems to act only as a structural part of the trans zigzag chain. This reflects the strong epitaxial interaction between the chain and the graphite surface compared with the interchain oxygen-oxygen interaction on these polyethers. However, the latter interaction is still effective, as the ether oxygen atoms are situated not randomly, but according to mutual shifting of neighboring chains by a regular amount.

Other Images. Even though most of images we have observed can be explained by the simple lattice rotational model, there are some images that do not fit. Figure 14 is an image of PTHF-I, but with an enhancement on every fifth chain. A defect on the graphite lattice or a compression of the polymer lattice on the β direction may be the cause. This is one example of a few cases where the moiré pattern cannot be explained by a simple rotation, even though the polymer structure can still be inferred.

In still other cases, some images exhibit well-defined patterns of an unknown structure. The image of POCB in Figure 15 has a distance between the fringes corresponding to the (0,7) relation. However, the distance between the parallel lines is 5.6 Å and every other line is enhanced. A high-resolution image does not help in identifying the spacing. Proceeding further requires additional assumptions on the image contrast, which are outside of the framework of the present fringe analysis.

It is difficult to predict both a moiré pattern and a polymer structure in the image of PEO shown in Figure 16. Every other line spaced 12 Å is enhanced and darker regions along the bright line are separated by 34 Å, corresponding to a 8×4.3 Å distance. Although the first effect can be produced by a bilayer construction of PEO-II layer on top of a PEO-III film, such a process can generate so many possibilities that a simple relation between the polymer structure and STM feature is lost.

This last comment has an implication that those images that could be accounted for by the present pattern analysis must be of a monolayer film on graphite. Since over 90% of the images obtained on the PTHF sample have been explained by the simple rotational model and the polymer images could be observed anywhere on this simple, we conclude that the graphite surface is covered almost completely by a molecularly thin film arranged with an epitaxial order.

Conclusion

In conclusion, the lattice rotational model is successfully applied to analyze the epitaxial structures of polyethers

on graphite. Due to the purely geometrical nature of this analysis, the same procedure can be applied to other epitaxially polymerized films for structural studies. Also, this study provides strong positive evidence for the assumptions made for the STM contrast. These assumptions may become a guideline to develop a quantitative theory for tunneling through organic adsorbates, which is required to predict detailed features of the molecular images. Polymerization-induced epitaxy combined with STM would allow us to investigate polymer interfacial phenomena on the atomic scale.

References and Notes

- (1) Sano, M.; Sasaki, D. Y.; Kunitake, T. *J. Chem. Soc., Chem. Commun.*, in press.
- (2) Mauritz, K. A.; Baer, E.; Hopfinger, A. J. *J. Polym. Sci., Macromol. Rev.* 1978, 13, 1-61.
- (3) Wittmann, J. C.; Lotz, B. *Prog. Polym. Sci.* 1990, 15, 909-948.
- (4) Swei, G. S.; Lando, J. B.; Rickert, S. E.; Mauritz, K. A. In *Encyclopedia of Polymer Science and Technology*; Korschwitz, J. I., Ed.; Wiley: New York, 1986; Vol. 6, pp 209-225, and references therein.
- (5) Smith, D. P. E.; Hörber, J. K. H.; Binnig, G.; Nejoh, H. *Nature* 1990, 344, 641-644.
- (6) McGonigal, G. C.; Bernhardt, R. H.; Thomson, D. J. *J. Appl. Phys. Lett.* 1990, 57, 28-30.
- (7) Rabe, J. P.; Buchholz, S. *Science* 1991, 253, 424.
- (8) Foster, J. S.; Frommer, J. E.; Spong, J. K. *Proc. SPIE, Liquid Cryst. Chem. Appl.* 1989, 1080, 200-208.
- (9) Spong, J. K.; Mizes, H. A.; LaComb, L. J. Jr.; Dovek, M. M.; Frommer, J. E.; Foster, J. S. *Nature* 1989, 338, 137-139.
- (10) For instance, Odian, G. *Principles of Polymerization*, 2nd ed.; John Wiley & Sons: New York, 1981; pp 508-565.
- (11) Smith, S.; Hubin, A. J. *J. Macromol. Sci. Chem.* 1973, A7, 1399-1413.
- (12) Yamashita, Y.; Kozawa, S.; Hirota, M.; et al. *Makromol. Chem.* 1971, 142, 171.
- (13) (a) Dreyfuss, P. *Polytetrahydrofuran*. *Adv. Polym. Sci.* 1967, 4, 528. (b) Gurgiolo, A. E. *Rev. Macromol. Chem.* 1966, 1, 39.
- (14) (a) Sano, M.; Kunitake, T. *J. Vac. Sci. Technol. B* 1991, 9, 1137-1140. (b) Sano, M.; Sasaki, D. Y.; Isayama, M.; Kunitake, T. *Langmuir* 1992, 8, 1893-1902.
- (15) Baukema, P. R.; Hopfinger, A. J. *J. Polym. Sci., Polym. Phys. Ed.* 1982, 20, 399-409.
- (16) Tadokoro, H. *J. Polym. Sci. C* 1966, 15, 1-25.
- (17) Kakida, H.; Makino, D.; Chatani, Y.; Kobayashi, M.; Tadokoro, H. *Macromolecules* 1970, 3, 569-578.
- (18) Takahashi, Y.; Sumita, I.; Tadokoro, H. *J. Polym. Sci., Polym. Phys. Ed.* 1973, 11, 2113-2122.

Registry No. PTHF, 24979-97-3; POCB, 25722-06-9; PEO, 25322-68-3; graphite, 7782-42-5.